Sol−Gel Prepared Pt-Modified Oxide Layers: Synthesis, Characterization, and Electrocatalytic Activity

H. M. Villullas,*,† F. I. Mattos-Costa,‡ P. A. P. Nascente,§ and L. O. S. Bulhões‡

Departamento de Físico Química, Instituto de Química, Universidade Estadual Paulista, 14800-900, Araraquara - SP, Brazil, Departamento de Química, CMDMC-LIEC, Universidade Federal de São Carlos, C.P. 676, 13565-905, São Carlos - SP, Brazil, and Departamento de Engenharia de Materiais, Universidade Federal de São Carlos, 13565-905, São Carlos-SP, Brazil

Received January 17, 2006. Revised Manuscript Received August 23, 2006

Thin films of pure RuO_2 and IrO_2 and mixed $Ru_{0.5}Ir_{0.5}O_2$ oxide modified with Pt particles were prepared by a sol−gel method in the form of thin films of ~2 μm thickness on Ti substrates. Surface morphology of these Pt-modified oxides was examined by scanning electron microscopy and was found to exhibit a significant influence of the chemical composition of the oxide matrix. Element mapping showed homogeneous distribution of the metals. X-ray diffraction and X-ray photoelectron spectroscopy analyses showed that these films consist of metallic Pt particles dispersed in an oxide matrix. Cyclic voltammetry in acid solutions showed that the sol−gel prepared layers have relatively high Pt surface areas. The electrocatalytic activity of these materials toward the anodic oxidation of formaldehyde and methanol was compared in terms of onset potential and current density and was found to follow the sequence: $Pt-Ru_{0.5}Ir_{0.5}O_2/Ti > Pt-RuO_2/Ti > Pt-IrO_2/Ti$.

Introduction

Nanostructured materials and nanometer-sized particles are of increasing importance in different areas of science and technology because of the large available surface areas. The development of new materials with good catalytic properties and good stabilities is still needed to improve the efficiency of many technologically relevant processes. Among several others, the conversion of chemical energy into electricity in direct alcohol fuel cells (DAFC) requires materials with higher catalytic activities to improve the performance of the anodes that is required to achieve current densities adequate for practical applications. The synthesis of nanoparticles, that has gained increasing attention throughout the last several years, combined with the need of supported high surface area materials with good catalytic properties has led to the development of different methods of preparation of supported nanometer-sized metallic particles.[1−3] Nanoparticles of Pt and binary Pt alloys have been anchored or dispersed on a wide variety of substrates and matrixes such as carbon powders,[4,5] Nafion membranes,[6,7] polymers,[8−10] polymer−oxide nanocomposites,[11] three-dimensional organic matrixes,[12] and oxide matrixes.[13,14]

One of the central problems associated to the poor performance of anodes for DAFC is related to the blocking of active sites by reaction intermediates, such as CO. Several different catalytic materials, most of them containing Pt with one or two other metals, have been proposed and the advances in their use in DAFC were recently reviewed.[15] Several bimetallic systems such as Pt−Ru,[1,16,17] Pt−Sn,[17−19] Pt−Ni,[20,21] Pt−Mo,[19,22] and Pt−W[19,22] have been investigated

* Author to whom correspondence should be addressed. E-mail: mercedes@iq.unesp.br.
† Universidade Estadual Paulista.
‡ Departamento de Química, Universidade Federal de São Carlos.
§ Departamento de Engenharia de Materiais, Universidade Federal de São Carlos.

(1) Watanabe, M.; Uchida, M.; Motoo, S. *J. Electroanal. Chem.* **1987**, *229*, 395.
(2) Bonnemann, H.; Richards. R. M. *Eur. J. Inorg. Chem.* **2001**, *10*, 2455.
(3) Gonzalez, E. R.; Ticianelli, E. A.; Pinheiro, A. L. N.; Perez, J. Brazilian Patent, INPl-SP No. 0032l, 1997.
(4) Lizcano-Valbuena, W. H.; Paganin, V. A.; Gonzalez, E. R. *Electrochim. Acta* **2002**, *47*, 3715.
(5) Bonnemann, H.; Brinkmann, R.; Britz, P.; Endruschat, U.; Mortel, R.; Paulus, U. A.; Feldmeyer, G. J.; Schmidt, T. J.; Gasteiger, H. A.; Behm, R. J. *J. New Mater. Electrochem. Syst.* **2000**, *3*, 199.
(6) Watanabe, M.; Uchida, H.; Emori, M. *J. Phys. Chem. B* **1998,** *102*, 3129.
(7) Uchida, H.; Mizuno, Y.; Watanabe, M. *J. Electrochem. Soc.* **2002**, *149*, A682.
(8) Napporn, W. T.; Laborde, H.; Leger, J. M.; Lamy, C. *J. Electroanal. Chem.* **1996**, *404*, 153.
(9) Giacomini, M. T.; Ticianelli, E. A.; McBreen, J.; Salasubramanian, M. *J. Electrochem. Soc.* **2001**, *148*, A323.
(10) Chen, C. C.; Bose, C. S. C.; Rajeshwar, K. *J. Electroanal. Chem.* **1993**, *350*, 161.
(11) Rajesh, B.; Thampi, K. R.; Bonard, J. M.; Xanthapolous, N.; Mathieu, H. J.; Viswanathan, B. *Electrochem. Solid-State Lett.* **2002**, *5*, E71.
(12) Bonnemann, H.; Waldofner, N.; Haubold, H. G.; Vad, T. *Chem. Mater.* **2002**, *14*, 1115.
(13) Avalle, L.; Santos, E.; Leiva, E.; Macagno, V. A. *Thin Solid Films* **1992**, *219*, 7.
(14) Esplandiu, M. J.; Avalle, L. B.; Macagno, V. A. *Electrochim. Acta* **1995**, *40*, 2587.
(15) Lamy, C.; Lima, A.; LeRhum, V.; Delime, F.; Coutanceau, C.; Léger, J. M. *J. Power Sources* **2002**, *105*, 283.
(16) Gasteiger, H. A.; Markovic, N.; Ross, P. N.; Cairns, E. J. *J. Phys. Chem.* **1993**, *97*, 12020.
(17) Krausa, M.; Vielstich, W. *J. Electroanal. Chem.* **1994**, *379*, 307.
(18) Wang, K.; Gasteiger, H. A.; Markovic, N.; Ross, P. N. *Electrochim. Acta* **1996**, *41*, 2587.
(19) Gotz, M.; Wendt, H. *Electrochim. Acta* **1998**, *43*, 3637.
(20) Park, K.-W.; Choi, J.-H.; Kwon, B.-K.; Lee, S.-A.; Sung, Y.-E.; Ha, H.-Y.; Hong, S.-A.; Kim H.; Wieckowski, A. *J. Phys. Chem. B* **2002**, *106*, 1869.
(21) Choi, J.-H.; Park, K.-W.; Kwon, B.-K.; Sung, Y.-E. *J. Electrochem. Soc.* **2003**, *150*, A973.

10.1021/cm0601178 CCC: $33.50
Published on Web 10/18/2006

and, so far, the best results have been obtained for Pt−Ru materials, which have been prepared in various ways such as alloys, electrodeposits, adsorbed Ru on Pt single crystals, carbon supported, and so forth.[1,4,5,16,17,23−32] It is currently accepted that the role of the second component is to provide oxygenated species that promote CO oxidation at lower potentials through a Langmuir−Hinshelwood reaction (bifunctional mechanism). However, the present knowledge of the nature of such oxygenated species is still rather incomplete.

Dispersion of Pt particles into an oxide matrix can lead, depending mainly on the oxide nature, to a Pt-modified oxide with better catalytic properties than pure Pt.[33−40] For instance, Pt−WO_x nanophases have shown an enhanced activity for the oxidation of methanol,[37] while a significant enhancement for CO and methanol oxidation was reported for electrodeposited Pt nanoparticles on IrO_2 films.[38] Some of us have shown that samples of different compositions containing Pt nanoparticles dispersed on RuO_2 layers also present a considerable activity for methanol oxidation.[39] Good electrocatalytic properties toward methanol oxidation was also recently reported for Pt−RuO_2 prepared by thermal decomposition of chlorides onto a Ti mesh[41] and for Pt nanoparticles supported on hydrous ruthenium oxide.[42]

While materials for methanol oxidation are currently the subject of numerous investigations, the oxidation of formaldehyde has been considered to a much lesser extent, despite the fact that formaldehyde is an intermediate or a product in methanol oxidation.[43,44] Some studies on metal single crystals,[45−49] on Pt−Ag and Pt−Au alloys,[50] and on DSA type electrodes[51] have been reported. A significant electrocatalytic activity toward the oxidation of formaldehyde was recently observed on Pt-modified SnO_2 layers prepared by a sol−gel method.[52]

In this work, Pt particles dispersed on pure RuO_2 and IrO_2 oxides and on a binary mixed oxide $Ru_{0.5}Ir_{0.5}O_2$ were prepared as thin layers by a sol−gel method. Theses materials were characterized by scanning electron microscopy (SEM), X-ray diffraction (XRD), and X-ray photoelectron spectroscopy (XPS) and their catalytic activity toward the anodic oxidation of formaldehyde and methanol was evaluated by cyclic voltammetry and current−time experiments.

Experimental Section

Preparation of the Pt-Modified Oxide Layers. Pt−RuO_2, Pt−IrO_2, and Pt−$Ru_{0.5}Ir_{0.5}O_2$ were prepared by a sol−gel method[53,54] in the form of thin films grown on titanium substrates, following a procedure similar to that described elsewhere.[55] Briefly, the sols were prepared by dissolving the precursors, hexachloroplatinic acid and ruthenium and iridium acetylacetonates (Aldrich), in isopropyl alcohol followed by the addition of adequate amounts of acetic acid. An ultrasonic treatment of a few minutes was done to ensure complete dissolution of the precursors and stabilization of the colloidal suspension. The sols were prepared keeping constant the nominal amount of Pt (40% in metal atoms). Thus, the nominal compositions of the samples used in this work were Pt:Ru 40:60, Pt:Ir 40:60, and Pt:Ru:Ir = 40:30:30. Ti plates of 1 cm^2 geometric area were sand-blasted, cleaned in a hot oxalic acid solution, rinsed, and dried prior to use. The sols were brushed on the Ti substrates under a flux of hot air to promote the gelation of the colloidal suspension (sol) and the drying of the gel (i.e., removal of residual organics and water) that leads to the xerogel state. The xerogel film obtained was subsequently heated in a furnace for 5 min. This procedure was repeated until a nominal thickness of about 2 μm, estimated from the deposited mass, was reached. A final annealing was carried out during 2 h at 400 °C, in air, to promote the removal of unreacted organic residues and the decomposition of the polymeric chains yielding the final material. Stabilization, densification, and introduction of crystallinity can also take place during this final heat treatment.

Characterization Techniques. XRD measurements were done with an X-ray diffractometer Rigaku model D Max 2500 PC using

(22) Oliveira-Neto, A.; Perez, J.; Napporn, W. T.; Ticianelli, E. A.; Gonzalez, E. R. *J. Braz. Chem. Soc.* **2000**, *11*, 39.
(23) Gasteiger, H. A.; Markovic, N.; Ross, P. N.; Cairns, E. J. *J. Electrochem. Soc.* **1994**, *141*, 1795.
(24) Markovic, N.; Gasteiger, H. A.; Ross, P. N.; Jiang, X. D.; Villegas, L.; Weaver, M. J. *Electrochim. Acta* **1995**, *40*, 91.
(25) Arico, A. S.; Poltarzewski, Z.; Kim, H.; Morana, A.; Giordano, N.; Antonucci, V. *J. Power Sources* **1995**, *55*, 159.
(26) Chrzanowski, W.; Wieckowski, A. *Langmuir* **1998**, *14*, 1967.
(27) Chrzanowski, W.; Kim, H.; Wieckowski, A. *Catal. Lett.* **1998**, *50*, 69.
(28) Kabbabi, A.; Faure, R.; Durand, R.; Beden, B.; Hahn, F.; Leger, J. M.; Lamy, C. *J. Electroanal. Chem.* **1998**, *444*, 41.
(29) Kelley, S. C.; Deluga, G. A.; Smyrl, W. H. *Electrochem. Solid-State Lett.* **2000**, *3*, 407.
(30) Iwasita, T.; Hoster, H.; John-Anacker, A.; Lin, W. F.; Vielstich, W. *Langmuir* **2000**, *16*, 522.
(31) Hoster, H.; Iwasita, T.; Baumgartner, H.; Vielstich, W. *Phys. Chem. Chem. Phys.* **2001**, *3*, 337.
(32) Kardash, D.; Korzeniewski, C.; Markovic, N. *J. Electroanal. Chem.* **2001**, *500*, 518.
(33) Tseung, A. C. C.; Chen, K. Y. *Catal. Today* **1997**, *38*, 439.
(34) Shen, P. K.; Tseung, A. C. C. *J. Electrochem. Soc.* **1994**, *141*, 3082.
(35) Lasch, K.; Jorissen, L.; Garche, J. *J. Power Sources* **1999**, *84*, 225.
(36) Jusys, Z.; Schmidt, T. J.; Dubau, L.; Lasch, K.; Jorissen, L.; Garche, J.; Behm, R. J. *J. Power Sources* **2002**, *105*, 297.
(37) Park, K. W.; Ahn, K. S.; Nah, Y. C.; Choi, J. H.; Sung, Y. E. *J. Phys. Chem. B* **2003**, *107*, 4352.
(38) Chen, A.; La, Russa, D. J.; Miller, B. *Langmuir* **2004**, *20*, 9695.
(39) Villullas, H. M.; Mattos-Costa, F. I.; Bulhões, L. O. S. *J. Phys. Chem. B* **2004**, *108*, 12898.
(40) Mello, R. L. S.; Mattos-Costa, F. I.; Villullas, H. M.; Bulhões, L. O.S. *Ecletica Quim.* **2003**, *28*, 69.
(41) Yang, L. X.; Allen, R. G.; Scott, K.; Christenson, P. A.; Roy, S. *Electrochim. Acta* **2005**, *50*, 1217.
(42) Chen, Z.; Qiu, X.; Lu, B.; Zhang, S.; Zhu, W.; Chen, L. *Electrochem. Commun.* **2005**, *7*, 593.
(43) Korzeniewski, C.; Childers, C. L. *J. Phys. Chem. B* **1998**, *102*, 498.
(44) Batista, E. A.; Malpass, G. R. P.; Motheo, A. J.; Iwasita, T. *Electrochem. Commun.* **2003**, *5*, 843.
(45) Adzic, R. R.; Avramovivic, M. L.; Tripkovic, A. V. *Electrochim. Acta* **1984**, *29*, 1353.
(46) Avramovivic, M. L.; Anastasijevic, N. A.; Adzic, R. R. *Electrochim. Acta* **1990**, *35*, 725.
(47) Adzic, R. R.; Wang, J. X.; Magnussen, O. M.; Ocko, B. M. *Langmuir* **1996**, *12*, 513.
(48) Olivi, P.; Bulhões, L. O. S.; Leger, J. M.; Hahn, F.; Beden, B.; Lamy, C. *Electrochim. Acta* **1996**, *41*, 927.
(49) Ramanauskas, R.; Jurgaitiené, I.; Vaskelis, A. *Electrochim. Acta* **1997**, *42*, 191.
(50) Stelmach, J.; Holze, R.; Beltowskabrzezinska, M. *J. Electroanal. Chem.* **1994**, *377*, 241.
(51) Motheo, A. J.; Gonzalez, E. R.; Tremiliosi-Filho, G.; Olivi, P.; de Andrade, A. R.; Kokoh, B.; Léger, J. M., Belgsir, E. M.; Lamy, C. *J. Braz. Chem. Soc.* **2000**, *11*, 16.
(52) Villullas, H. M.; Mattos-Costa, F. I.; Nascente, P.A.P.; Bulhões, L. O. S. *Electrochim. Acta* **2004**, *49*, 3909.
(53) Brinker, C. J.; Scherer G. W. *Sol gel science. The physics and chemistry of sol gel processing*; Academic Press: San Diego, CA, 1990.
(54) Lev, O.; Wu, Z.; Bhatathi, S.; Glezer, V.; Modestov, A.; Gun, J.; Rabinovich, L.; Sampath, S. *Chem. Mater.* **1997**, *9*, 2354.
(55) Villullas, H. M.; Mattos Costa, F. I.; Bulhões, L. O. S. *J. Electroanal. Chem.* **2003**, *545*, 89.

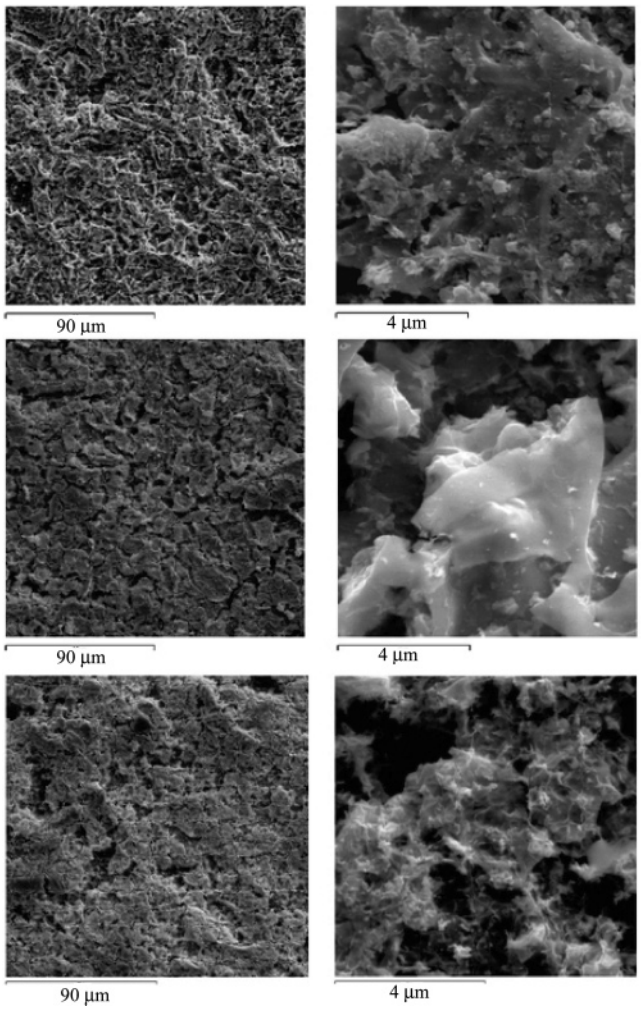

Figure 1. SEM micrographs of Pt−RuO_2/Ti (top), Pt−$Ru_{0.5}Ir_{0.5}O_2$/Ti (center), Pt−IrO_2/Ti (bottom).

a wavelength of 1.5406 Å (Cu Kα) and using a fixed incidence angle of 2°. A Zeiss DSM 94A equipment was used for the SEM study. The XPS analysis was performed in ultrahigh vacuum (low 10^{-7} Pa range) using a Kratos Analytical XSAM HS spectrometer. Al Kα ($h\nu = 1486.6$ eV) radiation was used as X-ray source, with emission of 10 mA at a voltage of 14 kV. The high-resolution spectra were obtained with analyzer energy of 20 eV. The accuracy of the electron analyzer is 0.1 eV. The binding energies were referred to the adventitious hydrocarbon C 1s line set at 284.8 eV. The Shirley background and the Gaussian and mixed Gaussian/Lorentzian functions and a least-square routine were used for fitting of the peaks. The sensitivity factors for quantitative analysis were referenced to SF1s = 1.0. In some cases, XPS analyses were performed before and after the electrochemical measurements.

All the electrochemical measurements were done in a conventional electrochemical cell, with a Pt foil counter electrode placed in a separate compartment and with a reversible hydrogen reference electrode. Solutions were prepared from analytical grade $HClO_4$ (Merck), formaldehyde (Mallinckrodt), analytical grade methanol (Mallinckrodt), and ultrapure water. All experiments were done at 25 °C in nitrogen-saturated solutions.

Results and Discussion

Morphology of the Sol−Gel Films. The influence of chemical composition on the surface morphology of the Pt-modified oxide films was examined by SEM. Figure 1 shows the SEM micrographs obtained for Pt−RuO_2/Ti, Pt−$Ru_{0.5}Ir_{0.5}O_2$/Ti, and Pt−IrO_2/Ti samples. The first observation is that none of these surfaces exhibit the "cracked mud" aspect typically observed for RuO_2,[56] IrO_2,[57] and RuO_2−IrO_2 mixtures[58,59] prepared at the same temperature. Although all three materials are rough and porous, the overall aspect of these samples is quite different and shows that the film composition has a significant effect on the general morphology. At low magnification (×500, left column), the surface of the Pt−$Ru_{0.5}Ir_{0.5}O_2$/Ti layer (center, left) has a flake-type aspect showing a significant number of small compact regions separated by deep cracks and holes. The surface of the Pt−RuO_2/Ti film (top, left) appears to have a spongelike structure while the Pt−IrO_2/Ti sample (bottom, left) presents a more or less continuous porous structure with relatively big holes in some regions. The micrographs obtained with higher magnification (×5000, right column) show the marked differences in the microstructure of these films. Qualitative analysis of film composition was done by energy-dispersive X-ray analysis (EDX) by integration of the dispersion peaks in the energy region of 0.1−10.3 keV. In a general manner, the results were in good agreement with nominal composition values. In addition, element mapping revealed a homogeneous distribution of the metals on the whole surface of all samples. Figure 2 shows an SEM micrograph and the corresponding Pt mapping for Pt on a Pt−RuO_2/Ti layer.

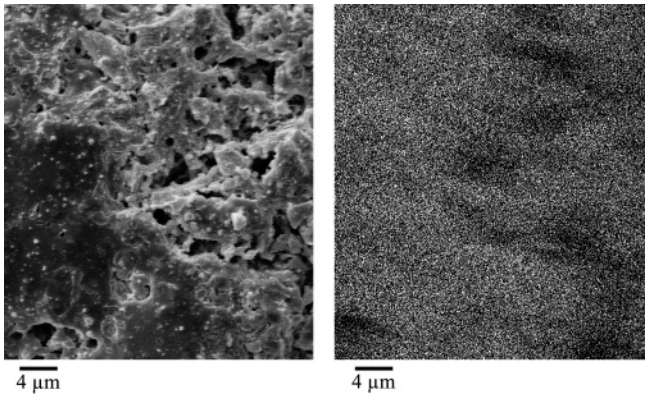

Figure 2. SEM micrograph (left) and Pt mapping (right) for the Pt−RuO_2/Ti sample.

Phase Composition of the Films. The phases present in the sol−gel prepared Pt-modified oxide films were identified by XRD. Figure 3 shows the diffraction patterns of Pt−RuO_2/Ti, Pt−$Ru_{0.5}Ir_{0.5}O_2$/Ti, and Pt−IrO_2/Ti samples. As it can be seen, the diffraction signals of the Ti substrate (JCPDS 44-1294) were observed in all the diffraction patterns of these thin films, even though a small-angle technique was used. For the Pt−RuO_2 layers (Figure 3a), the presence of RuO_2 is clearly evidenced by its most intense diffraction peak at $2\theta = 28°$ (JCPDS 43-1027). The characteristic peak of the Pt[200] planes at $2\theta = 46.2°$ (JCPDS 4-802) shows the presence of metallic Pt in the layer. It has been already demonstrated by XRD and XPS studies that sol−gel prepared

(56) Iwakura, C.; Sakamoto, K. *J. Electrochem. Soc.* **1985**, *132*, 2420.
(57) de Oliveira-Sousa, A.; da Silva, M. A. S.; Machado, S. A. S., Avaca, L. A.; de Lima-Neto, P. *Electrochim. Acta* **2000**, *45*, 4467.
(58) Kodintsev, I. M.; Trasatti, S.; Rubelt, M.; Wieckowski, A.; Kaufher, N. *Langmuir* **1992**, *8*, 283.
(59) Lin, S-M.; Wen, T-C. *J. Electrochem. Soc.* **1993**, *140*, 2265.

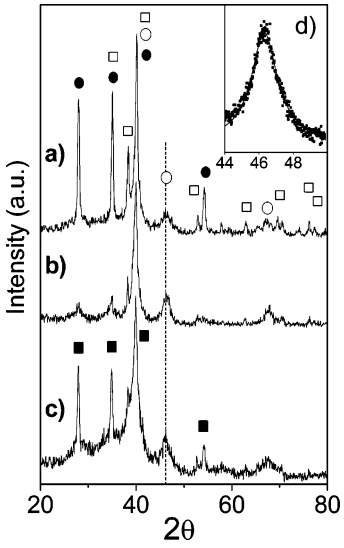

Figure 3. X-ray diffraction patterns: (a) Pt−RuO_2/Ti, (b) Pt−$Ru_{0.5}Ir_{0.5}O_2$/Ti, (c) Pt−IrO_2/Ti. Symbols: (white circle) metallic Pt; (black circle) RuO_2; (black square) IrO_2; (white square) Ti. The dashed line indicates the value $2\theta = 46.2°$ (see text). (d) Lorentzian fitting of the diffraction peak of the Pt [200] planes (Pt−$Ru_{0.5}Ir_{0.5}O_2$/Ti sample).

layers of Pt−RuO_2 densified in air do not contain either a Pt−Ru alloy phase or metallic Ru.[39] The peaks observed in the diffractograms of the Pt−$Ru_{0.5}Ir_{0.5}O_2$/Ti and Pt−IrO_2/Ti samples (Figure 3b and 3c) can be assigned to metallic Pt, RuO_2, and IrO_2 (JCPDS 43-1019) and to the Ti base, as indicated. No evidence of the presence of metallic Ir was found. For all three samples, the Pt characteristic peak of the [200] planes was observed at a 2θ value that coincides with the tabulated value of 46.2°, indicating the absence of alloys (Figure 3d). This Pt signal was used to calculate the average size of the Pt crystallites using Scherrer's equation.[60] Average crystallite sizes of about 28 nm for RuO_2 and of 6.8 nm for IrO_2 were calculated for the Pt−RuO_2/Ti and Pt−IrO_2/Ti samples, respectively, using the $2\theta = 28°$ signal. The calculated values agree well with those reported for sol−gel prepared nanoparticulated Pt[61] and for RuO_2 and IrO_2 layers.[62,63] For the Pt−$Ru_{0.5}Ir_{0.5}O_2$/Ti sample, the similarity of the lattice parameters for RuO_2 and IrO_2 does not allow determining from XRD analysis whether a mixed oxide or a solid solution was formed. Arikawa et al. studied RuO_2−IrO_2/Ti systems prepared by thermal decomposition of $RuCl_3$ and $IrCl_3$ by EXAFS and showed that RuO_2 forms a solid solution with IrO_2 for the binary oxide system.[64] Studies of sol−gel prepared RuO_2−IrO_2 ultrafine binary oxide particles also have shown that solid solutions are formed in a wide range of compositions and that the particle size was the smallest for the binary oxide with comparable Ru−Ir composition.[65] This might explain why the diffraction peak at 2θ of approximately 28° in the XRD pattern for Pt−$Ru_{0.5}Ir_{0.5}O_2$/Ti (Figure 3b) is wider and less intense than the peaks at the same 2θ value observed in the patterns for the Pt-modified pure RuO_2 and IrO_2 oxides. The average size of the oxide crystallites cannot be accurately calculated for the Pt−$Ru_{0.5}Ir_{0.5}O_2$/Ti sample. The obtained results are summarized in Table 1.

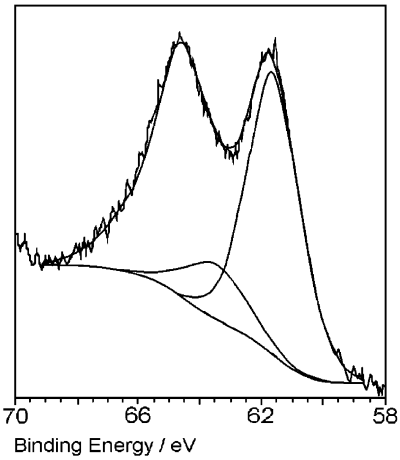

Figure 4. Ir 4f high-resolution XP spectrum for as-prepared Pt−IrO_2/Ti. (For clarity, only the fits for Ir $4f_{7/2}$ lines are shown.)

Table 1. XRD Derived Average Crystallite Sizes

	crystallite size (nm)	
sample	Pt	oxide
Pt−$Ru_{0.5}Ir_{0.5}O_2$/Ti	2.9	
Pt−RuO_2/Ti	4.2	28
Pt−IrO_2/Ti	4.8	6.8

Near-Surface Characterization. XPS analyses were initially performed on as-prepared samples. Wide-range XP spectra show no evidence of contamination with Ti or chloride. Detailed scans were recorded for the Ir 4f, Pt 4f, Ru 3d, O 1s, and C 1s regions. The Ir 4f XP spectra obtained for the two samples containing Ir (Pt−$Ru_{0.5}Ir_{0.5}O_2$/Ti and Pt−IrO_2/Ti) were almost identical. Figure 4 shows the Ir 4f XP spectrum for as-prepared Pt−IrO_2/Ti. The photoelectron lines observed are centered at 61.7 and 64.6 eV. The general shape of the spectrum presented in Figure 4 is very similar to that published by Kodintsev et al. for pure IrO_2 oxide prepared by thermal decomposition of chlorides on Ti (61.7 eV and 64.7 eV after 1 min sputtering).[58] For $Ru_xIr_{1-x}O_2$ mixed oxides, these authors reported binding energy values of 61.25−62.20 eV for Ir $4f_{7/2}$ and of 64.15−65.15 eV for Ir $4f_{5/2}$ signals, depending on composition and on sputtering conditions.[58] Deconvolution of the spectrum of Figure 4 shows two doublets. While the line with major intensity centered at 61.7 eV can be assigned to IrO_2, the photoelectron intensity above 63 eV can be interpreted as corresponding to hydrous speciation.[66,67] The binding energies for metallic iridium are 60.9 and 63.8 eV for Ir $4f_{7/2}$ and Ir $4f_{5/2}$, respectively.[66] Figure 4 shows no evidence of metallic Ir.

For all as-prepared samples, the Pt 4f XP spectra (not shown) revealed that significant amounts of metal oxide

(60) West, A. R. *Solid State Chemistry and Its Applications*; Wiley: Chichester, U.K.,1984.
(61) Andreas, H. A.; Birss, V. I. *J. Electrochem. Soc.* **2002**, *149*, A1481.
(62) Armelao, L.; Barreca, D.; Moraru, B. *J. Non-Cryst. Solids* **2003**, *316*, 364.
(63) Mattos-Costa, F. I.; de Lima-Neto, P.; Machado, S. A. S.; Avaca, L. A. *Electrochim. Acta* **1998**, *44*, 1515.
(64) Arikawa, T.; Takasu, Y.; Murakami, Y.; Asakura, K.; Iwasawa, Y. *J. Phys. Chem. B* **1998**, *102*, 3736.
(65) Murakami, Y.; Miwa, K.; Ueno, M.; Ito, M.; Yahikozawa, K.; Takasu, Y. *J. Electrochem. Soc.* **1994**, *141*, L118.
(66) Moulder, J. F.; Stikle, W. F.; Sobol, P. E.; Bomben, K. D. *Handbook of X-ray Photoelectron Spectroscopy*; Perkin-Elmer: Eden Prairie, MN, 1992.
(67) Rolison, D. R.; Hagans, P. L.; Swider, K. E.; Long, J. W. *Langmuir* **1999**, *15*, 774.

Table 2. Binding Energies of the Main Lines of the XP Spectra of As-Prepared Samples, Compared with Literature Values

	binding energies (eV)		
signal	published[58,62,66−68]	this work	assignment
Pt $4f_{7/2}$	71.2	71.8	metallic Pt
	73.8−74.2	73.6	Pt^{2+} (PtO)
	74.6−75.1	74.7	Pt^{4+} (PtO_2; $PtO_2.nH_20$)
Ru $3d_{5/2}$	279.9		metallic Ru
	281.0−281.2	281.1	RuO_2
	282.0−282.5	282.7	RuO_3 or hydrous speciation
	283.3	284	RuO_4 or hydrous speciation
Ir $4f_{7/2}$	60.9		metallic Ir
	62.1−63	61.7−61.9	Ir^{4+} (IrO_2)
		>63.5	hydrous speciation

species are present at the surface and were very similar to those previously found for Pt−RuO_2/Ti layers with different compositions.[39] Deconvolution of these spectra showed three doublets with binding energies of 71.4−71.8 eV, 72.7−73.6 eV, and 74.2− 74.7 eV. The first photoelectron line can be assigned to Pt in the zero-valence metallic state while the two other peak components can be attributed to Pt^{2+} and Pt^{4+} species.[66]

The Ru 3d + C 1s spectrum obtained for the as-prepared Pt−$Ru_{0.5}Ir_{0.5}O_2$/Ti sample was also very similar to that published for as-prepared Pt−RuO_2/Ti samples of different composition[39] and shows no evidence of the presence of metallic Ru on the surface. It was deconvoluted into three components with binding energies of 281.0, 282.4, and 283.8 eV. The line that has its major intensity centered at 281 eV can be attributed to RuO_2,[66] and it is in good agreement with published data for RuO_2[62] and RuO_2 containing mixtures[58] prepared by similar methods. The photoelectron intensity above 282 eV would correspond to Ru−O speciation[66] and can be assigned to either RuO_3 and RuO_4[68] or to hydrous speciation RuO_xH_y.[67] All these results are summarized in Table 2.

For all three samples, the O 1s photoelectron spectrum was composed of species with binding energies that can be attributed to oxide oxygen (530.1 eV, typical value of transition-metal oxides), to hydroxides (531.6 eV), and to hydration or adsorbed water (532.9 eV).[58] A Pt surface enrichment (∼10−20% higher than the nominal composition) was observed for all three samples.

Evaluation of Pt Surface Areas. The voltammetric curves obtained in 1 mol L^{-1} $HClO_4$ acid solution at 50 mV s^{-1} in the potential range of 0.05−0.8 V for as-prepared oxide films without Pt (RuO_2/Ti, $Ru_{0.5}Ir_{0.5}O_2$/Ti, and IrO_2/Ti) and for the Pt-modified oxides (i.e., Pt−RuO_2/Ti, Pt−$Ru_{0.5}Ir_{0.5}O_2$/Ti, and Pt−IrO_2/Ti) are shown in Figures 5 and 6, respectively. As it can be seen in Figure 5, the curves for the oxide films are essentially featureless showing little dependence of current on potential, in good agreement with published data.[39,69,70] It is well-established that hydrogenated species form on the surface of this oxides (RuO_2, $Ru_{0.5}Ir_{0.5}O_2$, and IrO_2) through

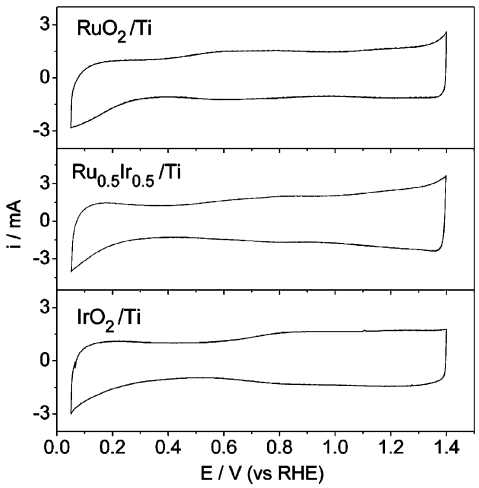

Figure 5. Voltammetric curves taken at 50 mV s^{-1} between 0.05 and 1.4 V for the oxide/Ti samples. Solution: 1 mol L^{-1} $HClO_4$.

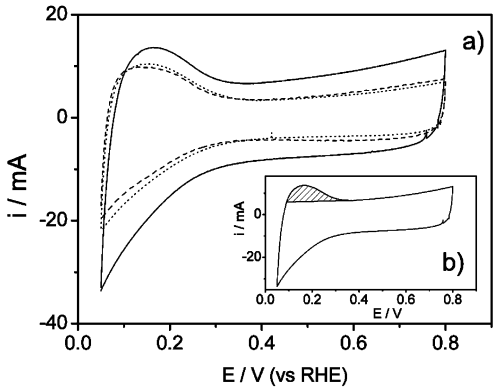

Figure 6. (a) Voltammetric curves taken at 50 mV s^{-1} between 0.05 and 0.8 V for Pt−$Ru_{0.5}Ir_{0.5}O_2$/Ti (——), Pt−RuO_2/Ti (- - - -), and Pt−IrO_2/Ti (. . . . .). Solution: 1 mol L^{-1} $HClO_4$. (b) Charge attributed to hydrogen desorption (shaded area), used for the calculation of the Pt surface area.

a process of electrochemical protonation[71]:

$$MO_2 + \delta H^+ + \delta e^- \leftrightarrow MO_{2-\delta}(OH)_\delta,\ 0 \le \delta \le 2 \quad (M = Ru \text{ or } Ir) \quad (1)$$

with the metal valence state increasing from $M^{2+}(OH)_2$ at about 0 V (vs SHE) to $M^{4+}O_2$ at about 1.4 V. Reaction 1 and its rate were experimentally determined for RuO_2 by tritium exchange experiments by Lodi et al.[72] The lack of clear evidence of any distinct redox couples in the curves (i.e., the transitions M^{2+}/M^{3+} and M^{3+}/M^{4+}) has been attributed to fully or partially delocalized electrons.[69,70,73] Additionally, the total charges involved in the cyclic voltammetries depend on the sample composition, following the sequence $Ru_{0.5}Ir_{0.5}O_2$/Ti > RuO_2/Ti ≅ Pt−IrO_2/Ti. This is, in fact, in good agreement with data reported in the literature for RuO_2+ IrO_2 films.[63,64,69,73] Such a dependence of the total charges upon the composition of $Ru_xIr_{1-x}O_2$ layers prepared on Ti plates has been reported in the literature for sol−gel prepared films[63] as well as for layers obtained by thermal decomposition of chloride solutions.[69,73] It was found that

(68) Liu, R.; Iddir, H.; Fan, Q.; Hou, G.; Bo, A.; Ley, K. L.; Smotkin, E. S.; Sung, Y. E.; Kim, H.; Thomas, S.; Wieckowski, A. *J. Phys. Chem. B* **2000**, *104*, 3518.
(69) Angelinetta, C.; Trasatti, S.; Atanasoska, Lj. D.; Atanasoski, R. T. *J. Electroanal. Chem.* **1986**, *214*, 535.
(70) Kötz, R.; Stucki, S. *Electrochim. Acta* **1986**, *31*, 1311.
(71) Trasatti, S.; Lodi, G. In *Electrodes of Conductive Metallic Oxides - Part A*; Trasatti, S., Ed.; Elsevier: New York, 1980; pp 301−358.
(72) Lodi, G.; Zucchini, G.; De, Battisti, A.; Sivieri, E.; Trasatti, S. *Mater. Chem.* **1978**, *3*, 179.
(73) Wen, T.-C.; Hu, C.-C. J. *Electrochem. Soc.* **1992**, *139*, 2158.

total voltammetric charge presents a maximum for x values around 0.5 (i.e., for nominal compositions close to $Ru_{0.5}Ir_{0.5}O_2$). For sol−gel prepared RuO_2-IrO_2 ultrafine particles, Murakami et al.[65] have shown that the binary oxide with comparable Ru−Ir composition had the smallest particle size.

The curves for the Pt-modified oxides (Figure 6) also exhibit total charges that depend on composition, following the same trend observed for the oxides without Pt. In the potential region up to ~0.35 V, all three curves show faradaic currents (anodic and cathodic). In a general manner, these curves are very similar to those published for Pt nanoparticles supported on carbon[4] and for Pt-modified SnO_2 oxide.[52]

To make a meaningful comparison of electrocatalytic activities of the different Pt-modified oxides, the current density at a given potential needs to be normalized by the true active area of Pt on the catalyst surface. The voltammetric curves of the oxides alone (Figure 5) show that a pseudocapacitance is, in principle, the only expected contribution of the oxide matrix in practically the whole potential window of Figure 6. Since hydrogen is not adsorbed on the oxides, it seems clear that the faradaic currents observed between 0.05 and ~0.35 V can only be associated to the processes of hydrogen adsorption and desorption on Pt. Thus, the anodic charge of the curves shown in Figure 6 was integrated up to ~0.35 V, after accounting for the double-layer contribution as indicated by the shaded area in Figure 6b. This integrated charge can be taken as due to desorption of hydrogen adsorbed on the Pt particles and can be used to estimate the Pt surface areas considering, as usual, that a monolayer of hydrogen involves a charge of ~210 μC/cm^2. Despite the significant differences in the general morphology of the Pt-modified oxide films (Figure 1), the estimated Pt surface areas turned out to be similar for all three samples (95, 92, and 102 cm^2 for Pt−RuO_2/Ti, Pt−$Ru_{0.5}Ir_{0.5}O_2$/Ti, and Pt−IrO_2/Ti, respectively).

Electrocatalytic Activity. Cyclic voltammograms for formaldehyde and methanol oxidation were obtained in the potential range between 0.05 and 0.9 V in 1 mol L^{-1} $HClO_4$ containing 0.5 mol L^{-1} formaldehyde or 0.5 mol L^{-1} methanol, respectively. Representative curves for the oxidation of formaldehyde obtained at 10 mV s^{-1} are shown in Figure 7a, for as-prepared Pt−RuO_2/Ti, Pt−$Ru_{0.5}Ir_{0.5}O_2$/Ti, and Pt−IrO_2/Ti. As it can be seen, all the curves for the oxidation of formaldehyde have more or less the same general shape. For Pt−RuO_2/Ti and Pt−IrO_2/Ti, the curves involve similar current densities, with a maximum at potentials of about 0.75 V. For Pt−$Ru_{0.5}Ir_{0.5}O_2$/Ti, the current density maximum appears at ~0.8 V, and the currents almost double those observed for the other two materials. Under identical experimental conditions, formaldehyde oxidation currents were not observed on the oxide/Ti samples. The initial portions of the curves (Figure 7b) show that the oxidation reaction begins at approximately 0.27 V on the two samples that contain RuO_2 while for Pt−IrO_2/Ti the onset potential is slightly shifted toward a more positive value. To compare electrocatalytic activities of different materials, not only the shape of the voltammetric profiles and the onset potentials but also the current densities at a fixed potential should be considered. Thus, current−time curves for the oxidation of formaldehyde were obtained at 0.5 V (Figure 7c).

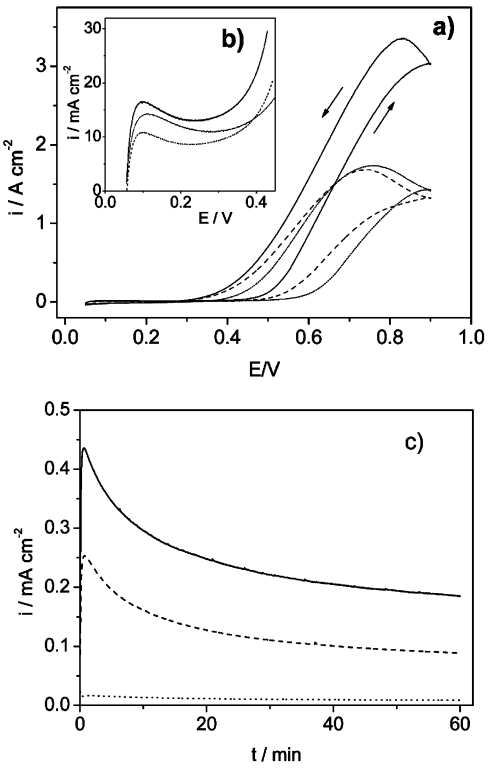

Figure 7. (a) Voltammetric curves taken at 10 mV s^{-1} between 0.05 and 0.9 V in 0.5 mol L^{-1} formaldehyde in 1 mol L^{-1} $HClO_4$ solution. Pt−$Ru_{0.5}Ir_{0.5}O_2$/Ti (——), Pt−RuO_2/Ti (- - - -), and Pt−IrO_2/Ti (. . . . .). (b) Enlarged initial portions of the voltammetric curves. (c) Current−time behavior for formaldehyde oxidation at 0.5 V. Current densities refer to Pt surface area calculated from H desorption charges (see text).

Some representative voltammetric curves for the oxidation of methanol obtained at a sweep rate of 10 mV s^{-1} are shown in Figure 8. The rise in current is initially faster for Pt−$Ru_{0.5}Ir_{0.5}O_2$/Ti, which exhibits the largest currents at potentials below ca. 0.6 V (which is the region relevant for fuel cell applications). The peak potential is almost the same for the two RuO_2 containing materials while for Pt−IrO_2/Ti it is shifted to more positive potentials. Figure 8b shows that methanol oxidation on Pt−RuO_2/Ti and Pt−$Ru_{0.5}Ir_{0.5}O_2$/Ti starts at about 0.3 V, while on Pt−IrO_2/Ti the onset of the reaction is shifted toward more positive potentials. There is also a significant difference in the shape of the initial portions of the oxidation curves, suggesting differences in the mechanisms operating in that potential region. Within the same potential region (0.05−0.9 V), methanol oxidation does not take place on the oxide/Ti samples. Figure 8c shows the current−time curves taken at 0.5 V for the three materials in 0.5 mol L^{-1} methanol solution.

For all three materials and both reactions, the peak current is proportional to the square root of the sweep rate, indicating that in the potential region of the current peak the oxidation of formaldehyde, as well as the oxidation of methanol, is controlled by diffusion. Similar results were reported by Honda et al. for methanol oxidation at boron-doped diamond films modified with Pt nanoparticles.[74]

(74) Honda, K.; Yoshimura, M.; Rao, Tata N.; Tryk, D.A.; Fujishima, A.; Yasui, K.; Sakamoto, Y.; Nishio, K.; Masuda, H. *J. Electroanal. Chem.* **2001**, *514*, 35.

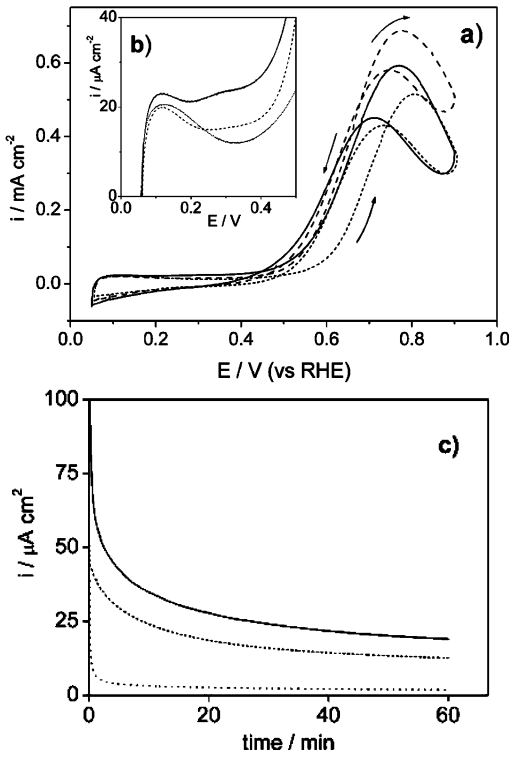

Figure 8. (a) Voltammetric curves taken at 10 mV s^{-1} between 0.05 and 0.9 V in 0.5 mol L^{-1} methanol in 1 mol L^{-1} $HClO_4$ solution. Pt−$Ru_{0.5}Ir_{0.5}O_2$/Ti (——), Pt−RuO_2/Ti (- - - -), and Pt−IrO_2/Ti (. . . . .). (b) Enlarged initial portions of the voltammetric curves. (c) Current−time behavior for methanol oxidation at 0.5 V. Current densities refer to Pt surface area calculated from H desorption charges (see text).

In all cases, a pronounced decay of the current is observed in the measurements at 0.5 V (Figures 7c and 8c). A similar loss of activity has been reported for smooth Pt−Ru catalysts[31,75,76] and for porous electrodes.[5] The reasons for this type of deactivation are still unclear, even though some authors have postulated that, in the case of alloys and other Pt−Ru catalysts, the current decay would be associated to the formation of RuO_2.[31]

The Role of the Oxide Matrix. As mentioned above, it is widely accepted that to oxidize the adsorbed CO formed during the oxidation of small organic molecules, such as formaldehyde and methanol, it needs to react with adsorbed OH species, through what is known as bifunctional mechanism:

$$(CO)_{ads} + (OH)_{ads} \rightarrow CO_2 + H^+ + e^- \qquad (2)$$

The better performance of Pt−Ru catalysts compared with Pt is attributed to the ability of Ru to dissociate water, that is, to form adsorbed OH, at lower potentials.

For all the samples studied in this work, a significant electrocatalytic activity for the oxidation of formaldehyde and methanol was observed. This could, in principle, be interpreted as associated to the formation of hydrogenated oxides on the surface of the oxide matrix that would be able to facilitate the conversion of CO to CO_2. The basis for this interpretation has been discussed in detail by Rolison et al.[67] and, more recently, by some of us.[39] The hydrogenated oxides $MO_{2-\delta}(OH)_\delta$ (see eq 1) are mixed electron/proton conductors. Also, they are able to dissociate water and have surface M−OH bonds. The conversion of CO to CO_2 could, in principle, be promoted by the $MO_{2-\delta}(OH)_\delta$ species taking place through a bifunctional mechanism, which in essence does not change if the oxygen donors are hydrous oxides. Thus, the CO adsorbed on the Pt particles could react with the OH species present at the oxide surface as in eq 2.

There are considerable differences, though, in the electrocatalytic activity of Pt−RuO_2/Ti, Pt−$Ru_{0.5}Ir_{0.5}O_2$/Ti, and Pt−IrO_2/Ti. While some significant activity is observed for Pt−RuO_2/Ti, a modest response is obtained for Pt−IrO_2/Ti. The results obtained for Pt−$Ru_{0.5}Ir_{0.5}O_2$/Ti evidence that the partial substitution of RuO_2 by IrO_2 produces a quite significant increase in current for the oxidation of formaldehyde (Figure 7) as well as for the methanol oxidation reaction (Figure 8).

It has been reported that below ca. 5 nm, the specific activity for methanol oxidation decreases with the decrease of Pt particle size.[77−79] Mukerjee and McBreen studied the role of the geometric parameters and the changes in the electronic structure due to adsorbates on methanol oxidation.[80] From XAS studies, they concluded that the combined effect of strongly adsorbed CO and OH on these small particles inhibits the oxidation of methanol. On the other hand, Kötz and Stucki[70] conducted a detailed XPS study of mixed oxides of the type $Ru_xIr_{1-x}O_2$ as a function of the composition *x*. From the shifts with composition *x* observed for the binding energy for the d-band derived t_{2g} band, they concluded that a common electronic d-band was formed in the mixed oxides.

The observed differences in electrocatalytic activity could, in principle, be associated to differences in the actual size of the Pt nanoparticles or to the chemical nature of the oxide matrix. Even though the actual Pt particle sizes and distribution cannot be determined for the Pt-modified oxides films, XRD data show that crystallite sizes vary in the range of 3−5 nm (see Table 1) while voltammetric curves indicated similar Pt surface areas. Thus, is seems unlikely that the substantial differences in electrocatalytic activity between the three materials studied in this work could be due exclusively to Pt particle size effects. The nature of the oxide matrix seems to have an important influence on the electrocatalytic properties. The electronic d-band of the oxides[70] may play a role in determining the ability of the hydrogenated oxide $MO_{2-\delta}(OH)_\delta$ to act as oxygen donor promoting the CO to CO_2 oxidation.

Surface Characterization after Polarization. Even though it is well-established that RuO_2 and IrO_2 do not reduce even in strongly reductive conditions such as polarization in the

(75) Waszczuk, P.; Solla-Gullón, J.; Kim, H.-S.; Tong, Y. Y.; Montiel, V.; Aldaz, A.; Wieckowski, A. *J. Catal.* **2001**, *203*, 1.
(76) Waszczuk, P.; Lu, G.-Q.; Wieckowski, A.; Lu, C.; Rice, C.; Masel, R. I. *Electrochim. Acta* **2002**, *47*, 3637.
(77) Kabbabi, A.; Gloagen, F.; Andolfatto, F.; Durand, R. *J. Electroanal. Chem.* **1994**, *373*, 251.
(78) Frelink, T.; Visscher, W.; van Veen, J. A. R. *J. Electroanal. Chem.* **1995**, *382*, 65.
(79) Takasu, Y.; Iwazaki, T.; Sugimoto, W.; Murakami, Y. *Electrochem. Commun.* **2000**, *2*, 671.
(80) Mukerjee, S.; McBreen, J. *J. Electroanal. Chem.* **1998**, *448*, 163.

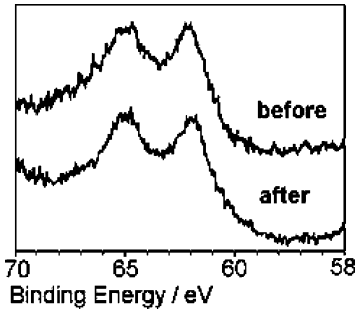

Figure 9. Ir 4f high-resolution XP spectra for Pt−$Ru_{0.5}Ir_{0.5}O_2$/Ti, before (as-prepared state) and after 60 min of polarization at 0.5 V.

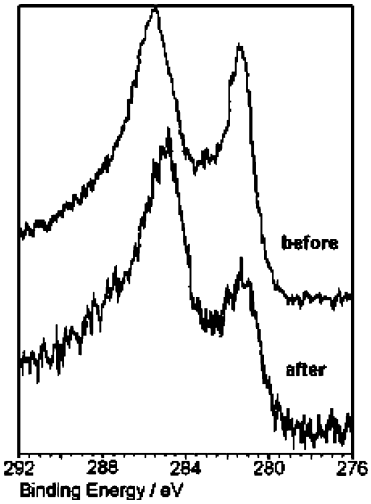

Figure 10. Ru 3d + C 1s high-resolution XP spectra for Pt−$Ru_{0.5}Ir_{0.5}O_2$/Ti, before (as-prepared state) and after 60 min of polarization at 0.5 V.

potential region of hydrogen evolution,[81−84] it might be important to determine whether or not metallic Ru or metallic Ir can be formed in the local reductive environment developed during the anodic oxidation of formaldehyde and methanol. With that purpose, XPS analyses were performed after the current−time experiments, that is, after polarizing the samples at 0.5 V during 60 min. In all cases, the XPS spectra remained almost unaltered. Figures 9 and 10 show the comparisons of the XP spectra of Ir 4f and Ru 3d, respectively, for Pt−$Ru_{0.5}Ir_{0.5}O_2$/Ti in the as-prepared state and after 60 min of methanol oxidation at 0.5 V. As shown in Figure 9, photoelectron lines centered at binding energy values of metallic iridium (60.9 and 63.8 eV, see above)[66] remain absent, indicating that iridium oxides were not reduced to metallic iridium during the experiments of methanol oxidation.

Similarly, comparison of the Ru 3d + C 1s XP spectra taken for the as-prepared state and after 60 min of methanol oxidation at 0.5 V (Figure 10) show that the photoelectron lines are centered at about the same binding energy values. No signal that could be attributed to metallic Ru (279.9 eV)[66] is observed, indicating that ruthenium oxides were not reduced to metallic Ru during the measurements of methanol oxidation. Comparison of the Ru 3d + C 1s also shows a significant increase in the C 1s signal after the experiments of methanol oxidation. Altogether, the XPS results indicate that neither metallic Ir nor metallic Ru was formed on the surface during the electrochemical experiments.

Conclusions

Pt-modified oxides (pure RuO_2, IrO_2, and $Ru_{0.5}Ir_{0.5}O_2$ mixed oxide) prepared by a sol−gel method in the form of thin layers deposited onto Ti substrates are rough and porous. The surface morphology is highly influenced by the chemical nature of the oxide. The films formed in air at 400 °C are formed by 3−5 nm Pt crystallites dispersed in the oxide matrix and exhibit large Pt surface areas. XPS analyses evidenced that neither metallic Ru nor metallic Ir are present on the surface of as-prepared samples. These analyses also showed that neither ruthenium nor iridium oxides are reduced to the metallic state during electrochemical oxidation of formaldehyde and methanol. All three samples showed good catalytic properties for the oxidation of formaldehyde and methanol, following the sequence Pt−$Ru_{0.5}Ir_{0.5}O_2$/Ti > Pt−RuO_2/Ti > Pt−IrO_2/Ti. The good electrocatalytic activity of these Pt-modified oxides can be interpreted as being associated to the presence of hydrous oxides ($MO_{2-\delta}(OH)_\delta$) that would play the role of oxygen donor and promote the CO to CO_2 oxidation.

Acknowledgment. Thanks are due to the Brazilian Agencies Fundação de Amparo à Pesquisa do Estado de São Paulo (FAPESP) and to the Conselho Nacional de Desenvolvimento Científico e Tecnológico (CNPq) for financial support. We also thank Dr. Silvia S. Maluf for her assistance with the XPS measurements. FIMC thanks FAPESP for a research fellowship.

CM0601178

(81) Chabanier, C.; Irissou, E.; Guay, D.; Pelletier, J. F.; Sutton, M.; Lurio, L. B. *Electrochem. Solid-State Lett.* **2002**, *5*, E40.
(82) Blouin, M.; Guay, D. *J. Electrochem. Soc.* **1997**, *144*, 573.
(83) Rochefort, D.; Dabo, P.; Guay, D.; Sherwood, P. M. A. *Electrochim. Acta* **2003**, *48*, 4245.
(84) Chabanier, C.; Guay, D. *J. Electroanal. Chem.* **2004**, *570*, 13.